

# Relaxation and flow in linearly sheared two-dimensional foams

Matthias E. Möbius, Gijs Katgert and Martin van Hecke

Kamerlingh Onnes Lab, Universiteit Leiden, Postbus 9504, 2300 RA Leiden, The Netherlands

(Dated: November 12, 2018)

We probe the relation between shear induced structural relaxation and rheology in experiments on sheared two-dimensional foams. The relaxation time  $t_r$ , which marks the crossover to diffusive bubble motion, is found to scale non-trivially with the local strain rate  $\dot{\gamma}$  as  $t_r \sim t_0^{0.34} \dot{\gamma}^{-0.66}$ . Here  $t_0$  is the single-bubble relaxation time, which is four to seven orders of magnitude smaller than the inverse strain rate — nevertheless, the flow is not quasistatic. The non-trivial rheology of the foam is shown to be intimately linked to the scaling of  $t_r$ , thus connecting macroscopic flow and microscopic bubble motion.

PACS numbers: 47.57.Bc, 83.60.Fg, 83.80.Iz

Soft glassy materials, such as foams, emulsions, colloidal glasses and granular media, exhibit highly complex flows. On the local scale, rearrangements in these densely packed systems are erratic due to geometric frustration. Globally, the relation between strain rate  $\dot{\gamma}$  and stress  $\tau$  is generally non-linear, often taking a Herschel-Bulkley form:  $\tau = \tau_Y + c_1 \dot{\gamma}^\beta$ , where  $\tau_Y$  denotes the yield stress, and where the viscous stress  $\tau_V \equiv \tau - \tau_Y$  scales nontrivially with the strain rate  $\dot{\gamma}$  [1, 2, 3].

What is the connection between the global rheology and the microscopic rearrangements of these materials? For non-Brownian systems, the strain rate controls the dynamics, therefore a fruitful strategy is to characterize and compare the dependence of both stress and local relaxation events on the strain rate. Recent experimental and simulation work on sheared foams has uncovered rich dynamics on the bubble scale [4, 5, 6, 7, 8] that often shows a non-trivial dependence of relaxation time scales on the strain rate [5, 6, 9]. However, except for ordered foams [10], a quantitative connection between these time scales and the bulk rheology is still lacking.

In this Letter we establish a direct and quantitative connection between the strain rate dependencies of both the microscopic relaxation time  $t_r$ , which embodies the decorrelation time of the bubble motion, and the macroscopic viscous stress  $\tau_V$  in experiments on a sheared two-dimensional, disordered foam. This approach is similar in spirit to recent work on glassy systems where this connection has been probed [11, 12]

We measure the relaxation dynamics directly by imaging the bubble motion, while the non-trivial rheology of this material is determined from rheometric measurements [8, 13]. Figure 1 shows examples of the bubble trajectories in a top view of our experiment. The average flow profiles exhibit shear bands in our experiment [8, 14, 15, 16] and we employ these to study the statistics of bubble displacements over a range of timescales and for local strain rates spanning three decades.

First, we establish that, for a given local strain rate, the probability distributions of bubble displacements exhibit fat tails for short times, develop exponential tails for

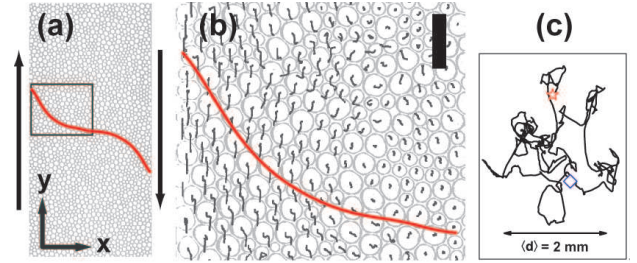


FIG. 1: (color online) (a) Schematic top view of the setup, with region of interest highlighted and typical flow profile indicated by the red curve. (b) Zoom of the highlighted region showing short time bubble trajectories. The width of the black bar denotes the bin size  $\Delta x = 1.6$  mm. (c) Example of a non-affine bubble trajectory over a period  $\Delta t = 145$  s, for  $\dot{\gamma} = 0.03$  s $^{-1}$ . The star and diamond symbol denote the starting and endpoint, respectively.

intermediate times and finally become Gaussian. The occurrence of purely exponential distributions at a sharply defined time allows us to extract the relaxation time  $t_r$ .

Second,  $t_r$  is not proportional with the inverse of the strain rate, which would be the simplest relation consistent with dimensional arguments, but instead exhibits a non-linear relationship with the inverse strain rate:  $t_r = (2.9 \pm 0.2) t_0^{1-\nu} \dot{\gamma}^{-\nu}$ , where  $\nu = 0.66 \pm 0.05$  and  $t_0$ , the single bubble relaxation time [17], equals  $1.3 \cdot 10^{-4}$  s.

Third, we find that the non-trivial scaling of the viscous stress with strain rate [8, 16] can be directly related to the scaling of the relaxation time:  $\tau_V = (0.83 \pm 0.05) G_0 \dot{\gamma} t_r$ , where  $G_0$  is the static shear modulus and the relaxation strain is defined as  $\gamma_r \equiv \dot{\gamma} t_r$ . In addition we show that this connection is consistent with a non-equilibrium Stokes-Einstein relation.

Our results firmly link strain rate, relaxation time, and stresses in two-dimensional foams. We stress, however, that our scenario is not particular to foams, and suggest to probe similar connections in other sheared, non-Brownian systems, such as suspensions, granular media, emulsions and microscopic models of these.

*Setup* — The measurements are performed in a linear shear cell (Fig. 1a) [8], in which we create a bidisperse

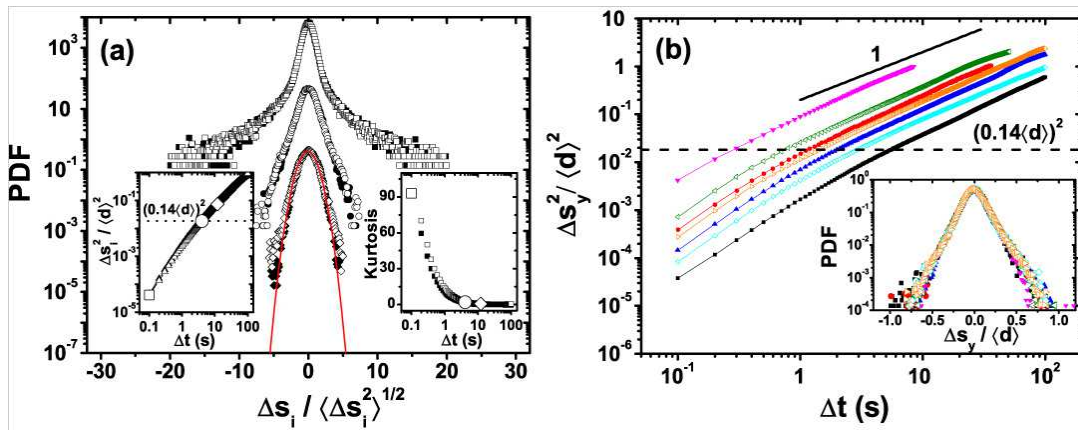


FIG. 2: (color online) (a) Evolution of transverse (full symbols) and longitudinal (open symbols) non-affine displacement PDF's at  $\dot{\gamma} = 0.005\text{s}^{-1}$ : (■, □) 0.1s; (●, ○) 4.1s; (◆, ◇) 12.1s. The PDF's are shifted for clarity and normalized by the width of the respective distributions. The red curve is a Gaussian distribution. Left inset: The corresponding longitudinal ( $\Delta$ ) and transverse ( $\blacktriangle$ ) mean square displacements as a function of time. Right inset: the Kurtosis  $\langle \Delta s_i^4 \rangle / \langle \Delta s_i^2 \rangle^2 - 3$  for the transverse (full symbols) and longitudinal (open symbols) fluctuations. In both insets the three symbols denote the time for which the PDF's have been plotted. (b) Mean square displacements  $\langle \Delta s_y^2 \rangle$  as a function of time at different local shear rates  $\dot{\gamma}$  in units of  $\text{s}^{-1}$ : (■) 0.002; (◇) 0.009; (▲) 0.016; (▷) 0.028; (●) 0.038; (◁) 0.11; (▼) 0.29. The horizontal line denotes the Lindemann criterion  $(0.14\langle d \rangle)^2$ . The inset shows the PDF's of the corresponding mean square displacements at the Lindemann criterion.

foam layer with bubble diameters of 1.7 and 2.7 mm in a soapy solution (5% volume fraction Dawn dishwashing liquid, 15% glycerol and 80% demineralized water, viscosity  $\eta = 1.8 \cdot 10^{-3} \text{ Pa}\cdot\text{s}$ , surface tension  $\sigma = 28 \cdot 10^{-3} \text{ N/m}$ ). The average bubble diameter  $\langle d \rangle$  equals  $2.0 \pm 0.1 \text{ mm}$ . The bubbles are trapped between the fluid layer and a glass plate placed 2.2 mm above the solution. Bubble coarsening is negligible over experimental time scales and we do not observe rupturing, coalescence or size separation of the bubbles. Local shear rates encountered in this experiment range from  $3 \cdot 10^{-4} \text{ s}^{-1}$  to  $0.3 \text{ s}^{-1}$ .

To induce shear, two rotating wheels of 39 cm diameter are partially immersed in a soap solution and spaced 7 cm =  $35 \langle d \rangle$  apart. The rotation speed of the wheels controls the driving velocity  $v_0$  of the shearing wall which we vary between 0.073 and 2.3 mm/s. The presence of the top glass plate causes shear banding [8, 14, 15] and a locally varying shear rate  $\dot{\gamma}(x)$ . We record the bubble motion by imaging the monolayer from above at 10 frames per second. Custom tracking software allows us to determine the bubble positions  $s_i$  to about  $0.005\langle d \rangle$ . We focus on a central region (Fig. 1a) where average flow transverse to the shear direction is absent:  $\langle v_x(x) \rangle = 0$ .

*Mean Squared Displacements* — In order to relate the rearrangement rate of the bubbles and the local strain rate, we divide the measurement area into bins of size  $\Delta x = 1.6 \text{ mm}$  (Fig. 1b), and determine for each the local average flow  $v(x)$  and shear rate  $\dot{\gamma} \equiv \partial v(x) / \partial x$ . We then determine the *non-affine* bubble tracks  $\Delta s_i(\Delta t)$  by subtracting the affine mean flow from the bubble trajectories  $s_i$ :  $\Delta s_i(\Delta t) \equiv s_i(t + \Delta t) - s_i(t) - \langle v_i(x) \rangle \Delta t$ . An example of an erratic bubble trajectory  $\Delta s_i$  is shown in Fig. 1(c). We only consider the mean square displace-

ments on short time scales where  $\sqrt{\langle \Delta s_i^2 \rangle} \lesssim \langle d \rangle$ , so that Taylor dispersion is negligible.

In Fig. 2(a), the probability distribution functions (PDF's) of both the  $x$  and  $y$  component of  $\Delta s$  are shown for a given local strain rate  $\dot{\gamma}$  at three different times as indicated in the left inset of Fig. 2(a). The fluctuations of the bubble trajectories are isotropic, and we normalize the widths of all distributions by  $\sqrt{\langle \Delta s_i^2 \rangle}$  to highlight the qualitative changes in these PDF's with time. For short times, they exhibit “fat tails”, similar to the instantaneous velocity fluctuations observed in a bubble raft [7]. Then, the PDF's develop exponential tails and eventually become Gaussian in the long time, diffusive regime. This behavior is also reflected in the evolution of the Kurtosis (inset Fig 2(a)). We note that the time at which the PDF's have exponential tails is well defined. This behavior should be contrasted to sheared glasses, where the PDF's were found to have exponential tails for a range of early times before crossing over to Gaussian behavior at late times [18, 19, 20].

In Fig. 2(b) we show the longitudinal mean square displacements for a range of local strain rates as function of time [21]. We find that the purely exponential PDF's occur when  $\Delta s_y^2 \approx (0.14\langle d \rangle)^2$ . This also holds for the transverse fluctuations [22]. Interestingly, this corresponds to the Lindemann criterion for melting in atomic solids and cage breaking in colloidal suspensions [11]. Here the relaxation time  $t_r$  marks the regime where the bubble motion crosses over from super-diffusive to diffusive (see Fig. 2(b)). Even though  $t_r$  can thus, in principle, be defined from the PDF's or from this crossover, for simplicity, we define  $t_r$  as the time where  $\Delta s_y^2 = (0.14\langle d \rangle)^2$ . Note that the non-affine bubble displacements between

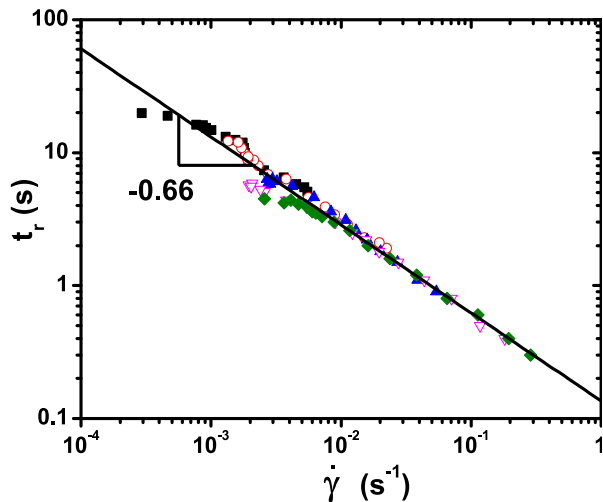


FIG. 3: (color online) Relaxation time as a function of local shear rate for different driving velocities: (■)  $v_0 = 0.076$  mm/s; (○)  $v_0 = 0.25$  mm/s; (▲)  $v_0 = 0.62$  mm/s; (▽)  $v_0 = 1.5$  mm/s; (◆)  $v_0 = 2.3$  mm/s.  $t_r$  is defined as  $\langle \Delta s_y^2 \rangle (\Delta t = t_r) = (0.14 \langle d \rangle)^2$ . The line is a fit to the data:  $t_r = 2.9 t_0^{0.34} \dot{\gamma}^{-0.66}$ .

rearrangements are of similar magnitude (Fig. 1(c)).

*Relaxation time* — We now extract  $t_r$  for a range of local strain rates  $\dot{\gamma}$  [21]. Since Brownian fluctuations do not play a role, the rearrangements in the foam are entirely shear induced, and *a priori*  $\dot{\gamma}^{-1}$  would be a prime candidate for setting the relaxation time. In contrast, we find that  $t_r = 2.9 t_0^{1-\nu} \dot{\gamma}^{-\nu}$ , where  $\nu \approx 0.66 \pm 0.05$ , and  $t_0$  is the characteristic relaxation time of single bubbles  $\eta(d)/\sigma = 1.3 \cdot 10^{-4}$  s — see Fig. 3. This non-trivial scaling is our central result, and it is far from obvious how it can be obtained, if at all, from the local interactions of the bubbles.

*Data collapse for mean squared displacements* — We now use our findings to collapse the mean squared displacement curves onto a single master curve. Fig. 4(a) illustrates that the system is not quasistatic, since the non-affine mean square displacements do not simply scale with strain. In fact, Fig. 4(a) shows that for a given local average strain,  $\Delta s_y^2$  is larger in regions where the local strain rate is smaller — fluctuations thus increase for slower flows.

Fig. 4(b) shows that it is possible to obtain good data collapse by rescaling the time axis with the relaxation time. We then find a super-diffusive behavior with an initial slope  $\approx 1.7$  for short times. Since large displacements due to bubble rearrangements are observed even on the 0.1 s time scale with which we image the foam, we do not see a ballistic regime. At later times the bubbles become diffusive and the slope approaches 1. From the collapse shown in Fig. 4(b) we deduce that the diffusion constant  $D_y$  scales non-linearly with the shear rate  $\dot{\gamma}$  as  $D_y = (0.017 \pm 0.002) \langle d \rangle / t_r \propto \dot{\gamma}^\nu$ . Similar results are found for the transverse fluctuations [22].

*Rheology* — We will now establish a surprising relation between relaxation times and rheology. Fig. 5 illustrates that our 2D foams exhibit a non-trivial rheology, with the shear stress  $\tau$  equal to the sum of a yield stress  $\tau_Y$  and the rate dependent viscous stress  $\tau_V = c_1 \dot{\gamma}^\beta$  [8]. Remarkably, the macroscopic rheological exponent  $\beta$  and the microscopic relaxation time exponent  $\nu$  are related as  $\beta \approx \nu - 1$ .

This connection between the viscous stress  $\tau_V$  and  $t_r$  can be made intuitive by defining a relaxation strain  $\gamma_r$  as the product of relaxation time and strain rate. The relaxation strain is thus increasing with shear rate, which is consistent with observations by Rouyer et al. [23]. To convert this relaxation strain into a stress, we multiply it with the static shear modulus  $G_0$  which we measured to be  $\mathcal{O}(\sigma/\langle d \rangle)$  (see inset Fig. 5) consistent with Princen et al. [24]. As Fig. 5 shows,  $G_0 t_r \dot{\gamma}$  and the viscous stress  $\tau_V$  are equal up to a numerical factor of order one:  $\tau_V = 0.83 G_0 t_r \dot{\gamma}$ . Hence the non-trivial global rheology of our foams, and in particular the non-trivial power law scaling of the viscous stress [8], is deeply connected to the scaling of the relaxation time  $t_r$  with local strain rate.

*Stokes-Einstein Relation* — In previous numerical work on sheared foams, a non-equilibrium Stokes-Einstein relation was found to relate the product of diffusion constant, viscosity and bubble size to an energy scale obtained from fluctuations in the elastic energy [6, 25]. We show now that our connection between relaxation time and viscous stress may also be viewed from this perspective. Both the diffusion constant  $D_y$  and the plastic viscosity  $\eta_p \equiv \tau_V/\dot{\gamma}$  are strain rate dependent. However, the product of these quantities yields an energy scale that is constant in the experimentally accessible range of strain rates:  $E = D_y \eta_p \langle d \rangle \approx 7 \cdot 10^{-3} \sigma \langle d \rangle^2$ , consistent with the simulation results at low strain rates [25]. Since the elastic response of a single bubble can be modelled by a spring with a spring constant  $4\pi\sigma$ , the energy scale  $7 \cdot 10^{-3} \sigma \langle d \rangle^2$  corresponds to compressing a single bubble by  $\approx 0.04 \langle d \rangle$ , which appears reasonable [26].

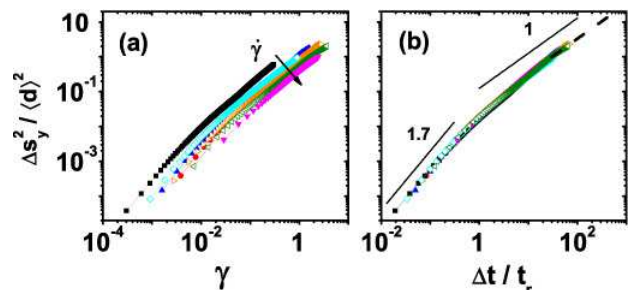


FIG. 4: (color online) (a) The non-affine mean square displacement  $\langle \Delta s_y^2 \rangle$  versus local strain  $\gamma = \dot{\gamma} \Delta t$  for different local shear rates (same data as Fig. 2(b)). (b) Same data as in (a), but plotted versus dimensionless time  $\Delta t/t_r(\dot{\gamma}) \propto (\Delta t/t_0)^{0.34} \dot{\gamma}^{0.66}$ . The dotted line indicates the diffusive limit:  $\langle \Delta s_y^2 \rangle = 2D_y \Delta t$ , with  $D_y = (0.017 \pm 0.002) \langle d \rangle^2 / t_r(\dot{\gamma})$ .

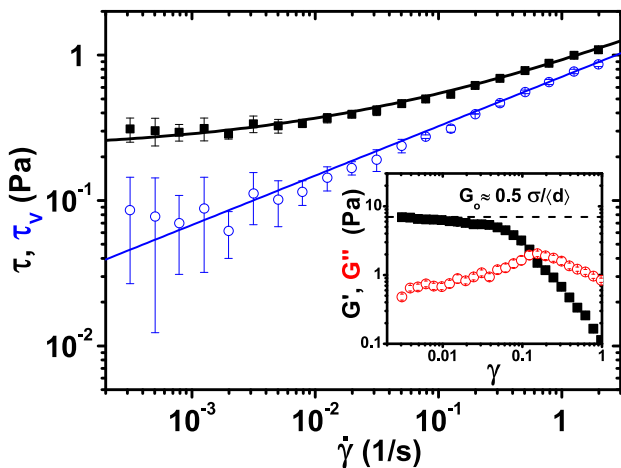


FIG. 5: (color online) Foam rheology. The stress is plotted as a function of shear rate measured in a Couette cell with inner radius 5 cm and outer radius 7 cm. The disordered foam is floating on the soap solution without the top plate and the boundaries have grooves to prevent bubble slip. The shear rate at the inner rotating wheel has been determined by image velocimetry. (■) total stress. The Herschel-Bulkley exponent is  $\beta = 0.36 \pm 0.05$ . The curve through the data is  $G_0 (\gamma_Y + 0.83 t_r \dot{\gamma})$ ; (○) viscous stress  $\tau_V \equiv \tau - \tau_Y$  where  $\tau_Y = 0.22 \pm 0.2$  Pa. The curve through the data is  $0.83 t_r \dot{\gamma}$ . Inset: Oscillatory strain sweep at 0.1 Hz.  $G'$  approaches the static shear modulus  $G_0$  at low strain amplitude:  $G_0 \approx 7$  Pa and the static yield strain  $\gamma_Y = 0.031$ .

*Discussion* — Our central result is the scaling of the relaxation time scales with strain rate:  $t_r \approx t_0^{1-\nu} \dot{\gamma}^{-\nu}$ . Defining quasistatic flows as those for which the precise bubble trajectories are independent of the flow rate, the nontrivial scaling of  $t_r$  and Fig. 4a and 4b clearly show that our flows are inconsistent with a quasistatic picture, even though the global stresses approach rate independence for slow flows. The microscopic scenario which emerges is that for increasingly slow flows, the delicate balance between elastic and viscous forces [27] causes the (relative) bubble motion to become increasingly concentrated in short bursts, such that the contribution of viscous forces to the averaged stress vanishes — leading to rate independence of the stress [8]. This scenario is consistent with the growth of  $\Delta s_y^2$  at fixed strain for decreasing  $\dot{\gamma}$  (Fig. 4a), and also with the absence of a ballistic regime (Fig. 4b): snapshots of the displacement fields over a finite time interval reveal strong spatially and temporally intermittent behavior, down to the shortest timescale that we have probed.

Finally, it may seem counter-intuitive that our system is not quasistatic, given that the single bubble relaxation time  $t_0$  [17] is several orders of magnitude smaller than the typical inverse strain rate in our system. However, the fluid flow is concentrated in the thin liquid films separating the bubbles. The shear rate in these films is therefore much closer to  $1/t_0$ , and the effective viscosity of the foam is much higher than the viscosity of the fluid phase

[10, 28].

*Acknowledgements* — The authors wish to thank J. Mesman for technical assistance, and discussions with R. Besseling, T. Witten and W. van Saarloos are gratefully acknowledged. GK and MM acknowledge support from physics foundation FOM, and MvH acknowledges support from NWO/VIDI.

- 
- [1] R. G. Larson, *The Structure and Rheology of Complex Fluids* (Oxford University Press, New York, 1999).
  - [2] R. Höhler and S. Cohen Addad, *J. Phys. Condens. Matter* **17**, R1041 (2005).
  - [3] D. Weaire and S. Hutzler, *The Physics of Foams* (Clarendon Press, Oxford, 1999).
  - [4] A. D. Gopal and D. J. Durian, *Phys. Rev. Lett.* **75**, 2610 (1995).
  - [5] A. D. Gopal and D. J. Durian, *J. Colloid Interface Sci.* **213**, 169 (1999).
  - [6] I. K. Ono, S. Tewari, S. A. Langer and A. J. Liu, *Phys. Rev. E* **67**, 061503 (2003).
  - [7] Y. Wang, K. Krishan and M. Dennin, *Phys. Rev. E* **74**, 041405 (2006).
  - [8] G. Katgert, M. E. Möbius and M. van Hecke, *Phys. Rev. Lett.* **101**, 058301 (2008).
  - [9] A. D. Gopal and D. J. Durian, *Phys. Rev. Lett.* **91**, 188303 (2003).
  - [10] N.D. Denkov et al., *Phys. Rev. Lett.* **100**, 138301 (2008); S. Tcholakova et al., *Phys. Rev. E* **78**, 011405 (2008).
  - [11] R. Besseling, E. R. Weeks, A. B. Schofield, and W. C. K. Poon, *Phys. Rev. Lett.* **99**, 028301 (2007).
  - [12] F. Varnik and O. Henrich, *Phys. Rev. B* **73**, 174209 (2006).
  - [13] N. D. Denkov et al., *Colloids Surf. A* **263**, 129 (2005).
  - [14] E. Janiaud, D. Weaire, and S. Hutzler, *Phys. Rev. Lett.* **97**, 038302 (2006).
  - [15] Y. Wang, K. Krishan and M. Dennin, *Phys. Rev. E* **72**, 031401 (2006).
  - [16] V. J. Langlois, S. Hutzler and D. Weaire, *Phys. Rev. E* **78**, 021401 (2008).
  - [17] D. Durian, *Phys. Rev. Lett.* **75**, 4780 (1995).
  - [18] A. Tanguy, F. Leonforte and J. L. Barrat, *Eur. Phys. J. E* **20**, 355 (2006).
  - [19] A. Lemaître and C. Caroli, *Phys. Rev. E* **76**, 036104 (2007).
  - [20] P. Chaudhuri, L. Berthier and W. Kob, *Phys. Rev. Lett.* **99**, 060604 (2007).
  - [21] We have checked that our results only depend on the local strain rate by varying both the driving velocity  $v_0$  and location of the bin.
  - [22] M. E. Möbius, G. Katgert and M. van Hecke (in preparation).
  - [23] F. Rouyer, S. Cohen-Addad, M. Vignes-Adler, and R. Höhler, *Phys. Rev. E* **67**, 021405 (2003).
  - [24] H. M. Princen and A. D. Kiss, *J. Colloid Interface Sci.* **112**, 427 (1986).
  - [25] I. K. Ono et al., *Phys. Rev. Lett.* **89**, 095703 (2002).
  - [26] M.-D. Lacasse et al, *Phys. Rev. Lett.* **76**, 3448 (1996).
  - [27] A. Liu et al., *Phys. Rev. Lett.* **76**, 3017 (1996).
  - [28] T. Witten, private communication.